电子束焊接热输入对 Ti-24Al-15Nb-1.5Mo/TC11 双合金焊接接头组织和显微硬度的影响

高 峻, 姚泽坤, 刘莹莹
(西北工业大学 材料学院, 西安 710072)

摘 要: 利用 OM, SEM, 能谱分析和显微硬度等测试方法对 Ti-24Al-15Nb-1.5Mo/TC11 双合金焊接接头的显微组织特征及硬度进行了分析. 结果表明, 焊接热输入为 135 kJ/m 时, 焊缝熔合区柱状晶由均匀密集的 α′ 相针状马氏体和少量 α 相组成, 显微硬度平均值为 447 HV. 焊接热输入增大到 150 kJ/m 时, 熔合区 α′ 相明显减少, 焊缝 TC11 合金侧热影响区的短针状 α+β 组织变为粗大的长针状组织, Ti-24Al-15Nb-1.5Mo 热影响区的 β 晶粒变得更粗, 显微硬度平均值降为 402 HV. 这主要是因为增大热输入使焊缝合金元素含量的比例发生变化, 并且冷却速度下降使焊缝组织形态和分布改变, 最终导致显微硬度降低. 合金元素 Ti, Al, Nb 的含量在焊缝边界发生突变, 但在焊缝熔合区达到一个新的平衡.

关键词: 电子束焊接; 双合金; 热输入; 微观组织; 显微硬度
中图分类号: TG113.12 文献标识码: A 文章编号: 0253-360X(2009)07-0033-04

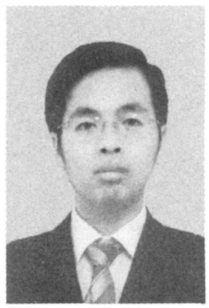

高 峻

0 序 言

改变发动机热端部件的材料或结构以提高压气机出口温度, 增大涡轮发动机的推重比, 进一步改善发动机的结构效益, 以适应大应力梯度和大温度梯度的工作环境, 是 Ti_3Al 基合金与钛合金双合金盘的研发目标[1]. 将轮缘和轮芯使用不同材料加工成整体的双合金盘, 能满足发动机转子系统整体设计和对使用性能的要求[2]. 而采用 Ti_3Al 基合金与(α+β)两相钛合金, 通过焊接+近等温成形技术, 制成轻质双合金盘(DAD)取代镍基高温合金做高压压气机盘或高压涡轮盘[3], 可显著提高飞机的推重比, 降低燃油比耗.

Ti_3Al 金属间化合物为密排六方有序 DO_{19} 超点阵结构, 具有密度低、比强度高、比模量高、高疲劳强度的特点, 在 600~750 ℃温度范围有可能替代高温合金[4-6]. TC11 两相钛合金具有良好的热强性和工艺性能. 这两种材料的热物理性能比较相近, 且都以钛为基, 以 Al 为主要的合金元素, 有较好的相容性, 满足异种材料焊接性要求. 因此, 研究电子束焊接参数对双合金焊接界面微观组织、显微硬度和合金元素扩散的影响, 分析了接头区域的微观组织特征和形成机理. 这对合理选择焊接工艺参数, 控制焊接双合金接头微观组织的变化, 推动双合金技术的应用, 具有重要的理论及现实意义.

1 试验方法

试验材料分别是 Ti-24Al-15Nb-1.5Mo 轧制棒和 TC11 棒材, 具体化学成分如表 1 所示.

表 1 试验材料主要化学成分(摩尔分数, %)

Table 1 Chemical composition of materials

	Al	Nb	Mo	Zr	Si	Ti
Ti-24Al-15Nb-1.5Mo	24.0	15.0	1.5	0	0	59.5
TC11	10.0~12.0	0	1.4~1.8	0.7~2.2	0.3~0.6	83.4~87.6

收稿日期: 2008-06-16
基金项目: 国家自然科学基金资助项目(50775187)

焊接试样尺寸为 φ20 mm×30 mm 的棒材. 焊接试验在德国制造的 EBOCAM KS55—G150—CNC 型

真空电子束焊机上完成，采用的焊接工艺参数见表 2. 焊后在焊接接头区域切取试样，制成金相试样. 腐蚀剂由 HF，HNO_3 和 H_2O，按体积比(0.5 ~ 1)∶3∶6 配成. 在光学显微镜及扫描电镜上观察了焊接接头的微观组织并测定合金元素含量. 进行显微硬度测定时，试验载荷 0.98 N，加载时间 15 s，焊接示意图见图 1.

表 2 试验用焊接工艺参数

Table 2 Experimental welding parameters

工艺	加速电压 U/ kV	聚焦电流 I_f/ mA	焊接电流 I_b/ mA	焊接速度 v/ (mm·s^{-1})	焊接热输入 E/(kJ·m^{-1})
Ⅰ	150	2 030	18	20	135
Ⅱ	150	2 030	20	20	150

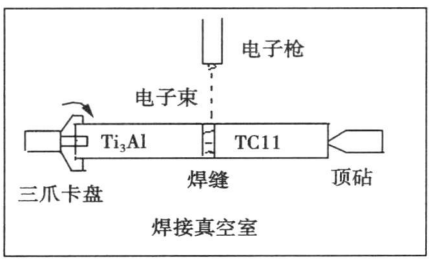

图 1 焊接示意图

Fig. 1 Schematic of welding

2 试验结果与分析

2.1 焊接热输入对焊缝组织的影响

由图 2a，b 可见，双合金电子束焊缝宏观形貌为颈部细长、杯口较小的高脚杯形状，其中部稍窄，整个焊缝以对接接头中心线对称分布，深宽比约为4∶1 以上，体现了电子束焊接深宽比大的特点，随着焊接热输入的增加，焊缝宽度有所增加. 这是由于电子束焊接能量密度高，加热速度快、熔化效率高使得形成的电子束焊缝呈细长而狭窄的条柱状[7]. 从图 2c，d 可以看出焊缝为典型的铸态组织，焊缝熔池内的凝固是从熔池边界开始的，是一种非均匀形核，焊缝金属呈柱状晶形式与母材连接. 当焊接热输入增大时，柱状晶的宽度明显增大，且在中部出现等轴晶. 晶粒从焊缝两侧基体合金开始外延结晶之后，晶体便呈柱状晶形式继续向焊缝内部成长. 焊缝形成这种结晶形态是因为液固界面处的最大温度梯度产生了最大凝固驱动力的缘故. 柱状晶的长大趋势各不相同，有的长大得很显著，一直延伸到焊缝中部；有的晶粒生长被抑制而呈短柱状，甚至有的未来得及生长.

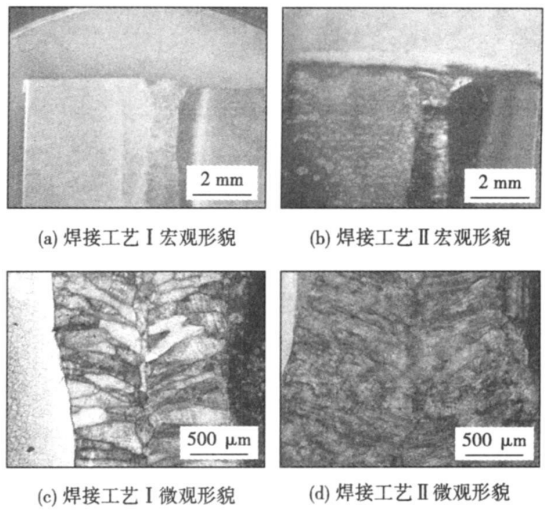

图 2 焊缝的组织形貌

Fig. 2 Optical micrographs of welded joints

图 3 为双合金焊件焊缝两侧母材、热影响区和焊缝的微观组织，明显可见 Ti-24Al-15Nb-1.5Mo 合金的母材为 B_2 相的基体上均匀的分布着等轴状的 α_2 相. TC11 钛合金的母材是由等轴和转变组织构成的双态组织(图 3a，b). 熔合区主要为胞状的凝固组织，通过 Ti-Al 相图及表 3 的焊缝合金元素能谱分析结果，认定其晶内为以 α，α_2，β 相和 β 转变组织为主的铸态混合组织(图 3e). Ti-24Al-15Nb-1.5Mo 侧热影响区最明显的特征是晶粒粗化，部分晶粒异常长大且形状不规则(图 3c). 这是因为在焊接过程中热影响区的温度远高于 β 相的转变温度，合金组织几乎完全变为 β 相，阻碍晶粒长大的 α_2 相粒子消失，晶粒长大的阻力大大降低，所以该区的晶粒长大十分明显[8]. TC11 侧热影响区的特点也是晶粒明显长大，但晶界较薄(图 3d). 在焊接过程中大部分 α 相转变为 β 相，β 相在高温下的长大速度很快，而且由于钛合金的导热性较差，促进了晶粒的长大. 在冷却过程中从 β 晶粒的晶界及晶内析出 α 或针状的 α′，所以该区是由 α 相、α′马氏体相和 β 相构成的混合组织. 虽然焊缝富集 Nb，Zr，Mo 等合金元素，但并未发现层状偏析现象.

表 3 焊缝能谱分析结果

Table 3 Result of energy spectrum analysis in welded joint

	Al	Ti	Zr	Nb	Mo
质量分数(%)	8.19	74.15	0.66	14.05	2.96
摩尔分数(%)	14.87	75.86	0.35	7.41	1.51

不同热输入时焊缝各个区域的 SEM 组织有着明显的差异. 在 TC11 侧的熔合线附近，即柱状晶起

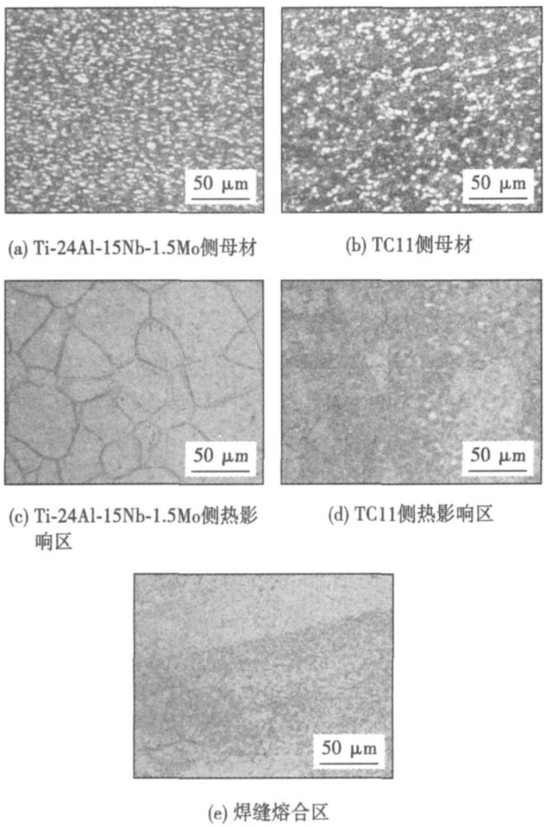

图 3　焊缝区域的微观组织

Fig. 3　Microstructure in welded joint

始处，如 1 号件热输入为 135 kJ/m 的热影响区组织为短针状的 α＋β 组织，没有观察到明显的晶界(图 4a)；而热输入为 150 kJ/m 的 2 号件虽然也是针状的α＋β 组织，却由于获得了更多的热能使 α 针粗化，且晶界明显(图 4b)．由于焊缝熔化金属的凝固速度很快，在快速冷却过程中，熔合区中 β 相析出 α 相的过程来不及完全进行[9]，但是 β 相的晶体结构变化却不易为冷却所抑制，仍然会发生改变．这种原始 β 相的成分未发生变化，但是晶体结构发生变化的过饱和固溶体是马氏体，即 α′．1 号件熔合区组织是原始相转变成的针状马氏体组织，组织十分均匀密集(图 4c)；2 号件组织中的针状马氏体数量比 1 号少，而且分布不均均，在部分区域比较集中，而且粗大的 β 晶粒已经形成(图 4d)．这可能是由于 2 号件的热输入增加，熔池冷却速度稍慢，部分 β 相转变为 α 相．

2.2　焊接热输入对显微硬度的影响

试验中发现焊接电流不同，焊缝的显微硬度差异较大，如图 5 所示．从图中可以看出，焊缝的显微硬度波动较大，熔合区的显微硬度高于两侧的热影响区，在 5 000 μm 处硬度值最高(HV0.98 为 5 003.2 MPa)．在 TC11 合金一侧，基体的硬度比较均匀，随

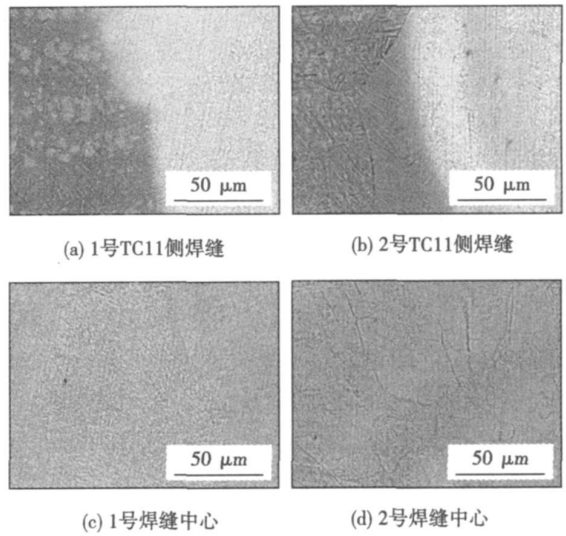

图 4　不同焊接工艺时焊接接头的 SEM 组织

Fig. 4　SEM microsgraphs of joints in different welding conditions

着进入热影响区深度加大显微硬度值先是有所下降，随后增加直到熔合区；进入 Ti-24Al-15Nb-1.5Mo 侧的热影响区后显微硬度开始下降，而且下降的速度较快．但靠近 Ti-24Al-15Nb-1.5Mo 基体处又有所上升，从而出现两个峰值区两个低谷区．仅在焊接热作用下合金元素扩散较弱，最后造成熔合区 Ti-24Al-15Nb-1.5Mo 侧的 Al 浓度高于 TC11 侧，Al 元素含量是形成金属间化合物硬相的决定因素，所以导致 Ti-24Al-15Nb-1.5Mo 一侧的硬度值偏高．

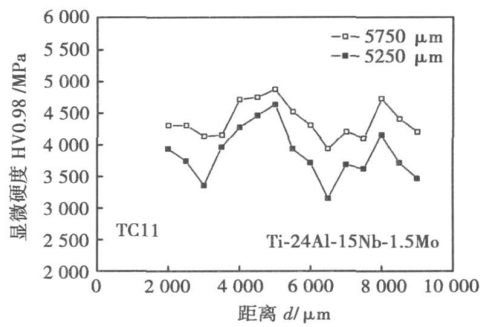

焊缝起点 4 250 μm→终点

图 5　Ti-24Al-15Nb-1.5Mo/TC11 焊缝区经不同工艺焊接后的显微硬度

Fig 5　Comparison of micro-hardness of different state Ti-24Al-15Nb-1.5Mo/TC11 weld samples

对比 1，2 号件，二者的显微硬度从 TC11 的热影响区到 Ti-24Al-15Nb-1.5Mo 的热影响区的变化趋势是基本相同的，但 1 号件在这一区域的显微硬度曲线整体位于 2 号的上方，硬度值 HV0.98 平均约为

4 466 MPa, 比 2 号件高出约 445 MPa. 这主要是因为不同的焊接热输入导致焊接后组织不同的结果, 1 号件 TC11 热影响区为短针状的 α+β 组织, 这种组织比 2 号件的长针状组织具有更多的相界[8], 所以该区硬度比 2 号件高. 在1 号件熔合区内的组织由密集的针状马氏体 α′构成, 而 2 号件的马氏体比较稀疏, 只有在某些区域比较集中. 1 号件这种单一的α′组织比 2 号件的 α+α′混合组织的硬度要高. 在 Ti-24Al-15Nb-1.5Mo 的热影响区内, 2 号件的β 晶粒比 1 号件要粗大的多, 单以颗粒大小作为基础, 一般而言, 大颗粒组织比小颗粒组织的硬度要低[9].

2.3 焊缝合金元素的分布

焊缝合金元素含量的能谱分布如图 6 所示. 从图中可以看到, Ti, Al, Nb 元素的含量在焊缝两侧的熔合线处发生突变, 坡度很陡. 然而, 各元素在熔合区与两侧热影响区内分布都比较均匀. Mo 元素在熔合线处的浓度虽有降低, 但因为 Mo 本身含量不高, 所以降低的比较平缓. Zr 元素在整个焊缝区的分布基本不变. 元素 Al, Nb 在焊接界面处的突然下降, 说明它们在该处基本没有发生扩散或扩散程度极小. 熔合区内所有元素的浓度都基本保持不变, 说明焊接过程中熔化的两种金属在电子束的搅拌作用下混合得较充分, 各元素分布比较均匀, 而且仅在焊接热作用下元素在熔合区内基本不发生扩散. 各元素难以发生扩散的原因除能量不足外, 还与熔合区主要是由针状马氏体构成有关, 因为合金元素很难通过这种六方或斜方晶格进行扩散.

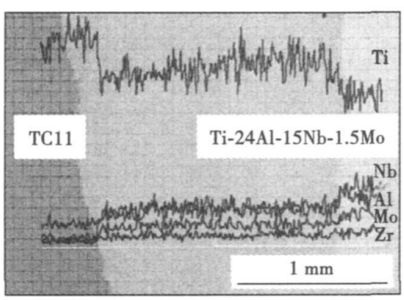

图 6 Ti-24Al-15Nb-1.5Mo/TC11 焊缝元素扩散的电子探针分析

Fig. 6 Result of electronic probe analysis for Ti-24Al-15Nb-1.5Mo/TC11 welding seam

表4 为焊缝熔合区不同位置的合金元素含量. 对比 1 号件和 2 号件, 1 号件熔合区的 Ti 含量比 2 号件平均低约 3%, Al 含量比 2 号件平均高约 0.6%, Nb 含量比 2 号件平均约高 3%. 这是因为随着焊接电流的增大, 更多的热输入使得更多的母材被熔化, 最终导致熔合区各元素比例发生变化. 根据元素增加和减小的情况可以断定, TC11 熔化量大于 Ti-24Al-15Nb-1.5Mo. 因为 1 号件熔合区的 Al 含量高, 在焊缝区会产生更多的 α_2 相; 此外, 1 号件熔合区的 Nb 含量比 2 号件高, 这使得 1 号件的 Ms 点更低, 所以 1 号件焊缝凝固过程中产生了更多的针状马氏体. 这是造成熔合区组织和显微硬度不同的根本原因所在.

表 4 焊缝熔合区不同位置的合金元素(质量分数, %)

Table 4 Content of elements in different sites of FZ

	1 号件焊缝中心距离 d_1/μm			2 号件焊缝中心距离 d_2/μm		
	−500	0	+500	−500	0	+500
Al	9.14	9.15	8.76	8.45	8.57	8.19
Ti	70.62	70.07	71.48	72.73	74.37	74.15
Zr	0.73	0.97	0.84	1.02	1.03	0.66
Nb	17.15	17.14	16.20	14.22	13.57	14.05
Mo	2.01	2.68	2.72	3.59	2.46	2.96

3 结 论

(1) 焊缝熔合区主要是 α_1, α_2 相和 β 转变组织构成的铸态混合组织, 两侧热影响区主要特征是晶粒粗大. 当焊接电流增大时, 熔合区内的针状马氏体数量减少, TC11 合金热影响区组织由短针状变为粗长针状.

(2) 焊缝的显微硬度波动较大, 熔合区的显微硬度高于两侧的热影响区, 硬度值最高达到 0.98 HV 时为 5 003.2 MPa. 焊接热输入较小时焊缝显微硬度整体高于焊接热输入较大时, 且硬度值平均高出 401 MPa.

(3) 合金元素 Ti, Al, Nb 的浓度在焊缝两侧的熔合线处发生突变, 但在两侧热影响区和熔合区内皆分布均匀, 且基本保持不变. 当焊接热输入较小时, Al, Nb 元素比焊接热输入较大时分别高出了 0.6%和 3%, 致使熔合区内 α_2 相增多, Ms 转变点降低, 针状马氏体的数量增加. 这是造成焊接热输入较小时焊缝显微硬度高的主要原因.

参考文献:

[1] 姚泽坤, 张梅琳, 梁新民, 等. 热力耦合作用对 TAC-1B 和 TC11 合金焊接界面硬度和显微组织的影响[J]. 焊接学报, 2004, 25(2): 125−128.
Yao Zekun, Zhang Meiling, Liang Xinmin, *et al*. The influence of heat and force coupling action on micro-hardness and microstructures at weld seam of TAC-1B/TC11 alloy[J]. Transactions of the China Welding Institution, 2004, 25(2): 125−128.

[下转第 40 页]

化合物长大,脆性层厚度增加,接头断裂仍发生在脆性层上,此时接头断口相组成主要为 Ti-Cu 二元金属间化合物 Cu_3Ti_2, $CuTi_2$, CuTi(图 5b),其中 Cu_3Ti_2 具有较好的塑性和韧性[8].

3 结 论

(1) 在最佳连接工艺参数下,TC4/ZQSn10-2-3 可以实现直接扩散连接,接头抗剪强度最大为 102 MPa,断口为脆性断口,发生在靠近 ZQSn10-2-3 侧.

(2) 在最佳连接工艺参数下,填加金属中间层铜,TC4/Cu/ZQSn10-2-3 扩散连接接头抗剪强度最大为 196 MPa,断口具有一定塑性,断口位于 TC4/Cu 侧.

(3) TC4/ZQSn10-2-3 直接扩散连接,由于接头中生成 $CuSn_3Ti_5$, Cu_3Ti 等金属间化合物及富集的铅,因而接头强度不高. 填加金属中间层铜,接头强度有了显著的提高,这是因为中间层铜有效地抑制了 Sn, Pb 向 TC4 侧的扩散. 因而可以判断 $CuSn_3Ti_5$ 以及富集的铅是造成接头强度不高的主要原因.

参考文献:

[1] Yao Wei, Wu Aiping, Zou Guisheng, *et al*. Formation process of the bonding joint in Ti/Al diffusion bonding[J]. Materials Science and Engineering A, 2008, 480: 456—463.

[2] Wang Juan, Li Yajianga, Liu Penga, *et al*. Microstructure and XRD analysis in the interface zone of Mg/Al diffusion bonding[J]. Journal of Materials Processing Technology, 2008, 205: 146—150.

[3] Nono M C A, Barroso J J, Castro P J. Mechanical behavior and microstructural analysis of alumina-titanium brazed interfaces[J]. Materials Science and Engineering A, 2006, 435—436: 602—605.

[4] Bhowmik S, Benedictus R, Poulis J A, *et al*. High-performance nanoadhesive bonding of titanium for aerospace and space applications [J]. International Journal of Adhesion & Adhesives, 2008, 29: 259—269.

[5] 刘 伟, 陈国庆, 张秉刚, 等. 钛/铜合金电子束焊接工艺优化[J]. 焊接学报, 2008, 29(5): 89—92.
Liu Wei, Chen Guoqing, Zhang Binggang, *et al*. Investigation on process optimization of Cu/Ti electron beam welding[J]. Transactions of the China Welding Insitution. 2008, 29 (5): 89—92.

[6] Robbiola L, Tran T T M, Dubot P, *et al*. Characterisation of anodic layers on Cu-10Sn bronze (RDE) in aerated NaCl solution[J]. Corrosion Science, 2008, 50: 2205—2215.

[7] Tavakoli A, Liu R, Wu X J. Improved mechanical and tribological properties of tin-bronze journal bearing materials with newly developed tribaloy alloy additive[J]. Materials Science and Engineering A. 2008, 489: 389—402.

[8] Kundu S, Chatterjee S. Effect of temperature on formation of reaction products and strength properties of titanium and stainless steel joints using copper interlayer[J]. Material Science and Technology, 2007, 23(3): 368—373.

作者简介:赵 贺,男,1978 年出生,博士研究生. 研究方向为异种材料连接. 发表论文 6 篇.

Email: zhaoh_join@sina.com

[上接第 36 页]

[2] 田世藩, 张国庆, 李 周, 等. 先进航空发动机涡轮盘合金及涡轮盘制造[J]. 航空材料学报, 2003, 23(增刊): 233—238.
Tian Shifan, Zhang Guoqing, Li Zhou, *et al*. The disk superalloys and disk manufacturing technologies for advanced aero engine[J]. Journal of Aeronautical Materials, 2003, 23(S1): 233—238.

[3] Gayda J, Furrer D. Dual-micro heat treat[J]. Advanced Materials & Processes, 2003, (10): 36—39.

[4] 邹彦如, 周光爵. Ti_3Al 基合金研究现状[J]. 稀有金属, 1991(4): 283—289.
Wu Yanru, Zhou Guangjue. Present situation of research on Ti_3Al alloy[J]. Rare Metals, 1991(4): 283—289.

[5] Shi Y W, Zhong F, Li X Y. Effect of laser beam welding on fracture toughness of a Ti-6.5Al-2Zr-1Mo-1V alloy sheet[J]. Materials Science, 2007, 42(16): 6651—6657.

[6] 张永刚, 韩雅芳, 陈国良, 等. 金属间化合物结构材料[M]. 北京: 国防工业出版社, 2001.

[7] 张秉刚, 冯吉才, 吴 林, 等. TiAl/TiAl 和 TiAl/TC4 真空电子束焊接头组织结构及焊接性[J]. 焊接, 2004(5): 14—16
Zhang Binggang, Feng Jicai, Wu Lin, *et al*. Study on weldability and microstructure of butt joints of TiAl/TiAl, TiAl/TC4 welded by EBW [J]. Welding & Joining, 2004(5): 14—16.

[8] Zhang H T, He P, Feng J C, *et al*. Interfacial microstructure and strength of the dissimilar joint Ti_3Al/TC4 welded by the electron beam process[J]. Materials Science and Engineering A, 2006, 425(1—2): 255—259.

[9] 吴会强, 冯吉才, 何景山. 电子束焊接热输入对 Ti-6Al-4V 组织结构的影响[J]. 焊接学报, 2004, 25(5): 41—44.
Wu Huiqing, Feng Jicai, He Jingshan. Effects of electron beam heat input mode on microstructure of Ti-6Al-4V[J]. Transactions of the China Welding Institution, 2004, 25(5): 41—44.

作者简介:高 峻,男,1980 年出生,工学硕士,助教. 主要从事钛基双合金盘研究工作. 发表论文 2 篇.

Email: gaojun@mail.nwpu.edu.cn

Key Laboratory of Gansu Advanced Non-Ferrous Metal Materials, Lanzhou University of Techenology, Lanzhou 730050, China; 2. Division of Strucrural Materials, Central Iron and Steel Research Institute, Beijing 100081, China). p 17—20

Abstract: Microstructure and mechanical properties of HAZ of 980 MPa low carbon bainite high strength steel joints were studied. The different regions of welded joint HAZ were simulated by welding thermal simulation technique. Microstructure observation, phase analysis, and corresponding tensile and impact test for different regions of welded joint HAZ were taken. The results indicate: the impact property of coarse grain zone is the best, while the impact property of fine grain zone is the worst. So the fine grain zone is the weakest part of the welded joint. Microstructure of coarse grain zone is uniform interweaved coarse and fine lath martensites, and precipitation acicular ferrite are distributed between the lath martensites. Toughness of coarse grain zone is increased owing to the austenite thin film adherent lath martensite interface. Microstructure of fine grain zone are twin martensite and a small number of lath maartensite, only minor acicular ferrite are distributed in the twin martensite. Toughness of fine-grained zone was decreased owing to twin martensite.

Key words: 980 MPa high strength steel; welding thermal simulation; heat affected zone; austenite film

The multi-information fusion quality judgment of spot welding based on rough sets LI Dongtao, PAN Cunhai, DU Sumei, GUO Shilin (College of Mechanical Engineering, Tianjin University of Science and Technology, Tianjin 300222, China). p 21—24

Abstract: The new method of quality judgment about on-line aluminum alloy spot welding was studied, which was based on the rough set theory. The eight characters selected from two parameters (electrode displacement and electrode force in the weld process) constituted the knowledge representation system. The new method dealt with the obtained information by adopting the discretized continuous attribute algorithm with the self-organizing feature map network (SOM) and the attribute reduction algorithm based on discernibility matrix, picked up the distinguish rule, then completed the classification of spot welding quality by the rule. The method can not only reduce the dimensions of the feature space, the workload of quality classification and the information memory capacity, but also can make the accuracy of the spot weld quality judgment reach 97.03%.

Key words: quality judgment; rough set; attribute discrimination; attribute reduction; resistance spot welding

Appearance of fine grain titanium alloy by tungsten iner-gas arc welding(GATW) ZHOU Shuiliang, TAO Jun, GUO Delun (Aeronautical Key Laboratory for Aviation Joining Technology, Beijing Aeronautical Manufacturing Technology Research Institute, Beijing 100024, China). p 25—28

Abstract: Fine grain titanium alloy is used extensively in aerospace and ailrraft because of its excellent comprehenslve properties and outstanding machinability. Fine grain Ti-6Al-4V alloy and common grain Ti-6Al-4V alloy were welded by tungsten iner-gas arc welding(GTAW) respectively. Welding parameters and appearance of two Ti-6Al-4V alloys welded were investigated. The results indicate that the heat conductivity impediment of grain boundary strengthened because of fine grain Ti-6Al-4V alloy grains refinement and grain boundary increasing. Thus, its coefficient of heat conductivity is decreasing. Camparing with appearance of common grain Ti-6Al-4V alloy, when the range of welding current parameter was wide, the appearance of fine grain Ti-6Al-4V alloy was bad. However, when the range of welding current parameters was narrow relatively, the appearance of fine grain Ti-6Al-4V alloy welded was better than the one of common grain Ti-6Al-4V alloy. The possible influencing factors were discussed. At last, according to the specimen size, an optimal welding current parameter(47～48)A was recommended.

Key words: fine grain Ti-6Al-4V alloy; appearance of weld; heat conductivity; grain boundary

Influence of TIG arc on characteristics of high power CO_2 laser beam ZHANG Huanzhen, WU Shikai, XIAO Rongshi (Institute of Laser Engineering, Beijing University of Technology, Beijing 100124, China). p 29—32

Abstract: By instruments such as the laser power meter, the beam diagnosis and the fast CCD camera, the effects of the DC TIG arc on the characteristics of a vertically incident CO_2 laser beam were investigated. The experimental results demonstrate that part of the laser beam energy is absorbed by the arc plasma. This absorption increases with the increase of the arc current and the incident laser power, and becomes more evident as the laser beam incident position is closer to the anode. Meanwhile, the laser beam will be defocused, deformed and deviated to the cathode due to the arc refraction. The beam defocusing, deformation and deviation become more obvious with increasing the arc current and the incident laser power, and impinging the laser beam closer to the anode. The combined effect of the absorption and defocusing causes the power density decreases sharply as the beam passes through the arc.

Key words: CO_2 laser; arc; absorption; refraction; negative lens

Effects of electron beam heat input on microstructure and micro-hardness of Ti-24Al-15Nb-1.5Mo/TC11 dual alloys GAO Jun, YAO Zekun, LIU Yingying (School of Materials, Northwestern Polytechnical University, Xi'an 710072, China). p 33—36, 40

Abstract: Microstructure evolution characterization of the Ti-24Al-15Nb-1.5Mo/TC11 dual alloys welded joints obtained on the condition of different electron beam heat input was studied by optical microscope, scanning electron microscope, energy spectrum and micro-hardness analysis. The results show that the energy input have an important effect on the microstructure, grain size, micro-hardness and alloy elements content of welded joints. The microstructure is made up of homogeneous acicular martensite α' phase in fusion zone

(FZ) and the average micro-hardness value is 447HV when heat input E= 135 kJ/m is utilized. With heat input increasing to 150 kJ/m, the number of α' phase decreases in FZ, short acicular $\alpha+\beta$ phase become coarser in heat-affected zone(HAZ) of TC11, coarse β grains become larger in HAZ of Ti-24Al-15Nb-1.5Mo and the average micro-hardness value drops to 402HV. The result is attributed to the changed content of alloy elements and lower cooling velocity caused by increasing heat input. The content of element Ti, Al and Nb is changed abruptly in the boundary of the joint, but these elements evenly distribute in each zone and hardly diffuse.

Key words: electron beam welding; dual alloy; heat input; fine texture; microstructure

Microstructural characterization of TC4/Cu/ZQSn10-2-3 diffusion bonded joints ZHAO He, CAO Jian, FENG Jicai (State Key Laboratory of Advanced Welding Production Technology, Harbin Institute of Technology, Harbin 150001, China). p 37—40

Abstract: The experimental investigation on the diffusion bonding of TC4 to ZQSn10-2-3 was carried out in vacuum. $CuSn_3Ti_5$, Cu_3Ti and rich-Pb layer were formed at the interface zone. The maximum joint strength was 102 MPa. Brittle fracture was explored after shear test, and occurred proximity to ZQSn10-2-3 side. Using copper as the interlayer, element Sn and Pb can be avoid diffusing from ZQSn10-2-3 to TC4. Then there were little $CuSn_3Ti_5$ in the interface. Fracture had certain plasticity, and the maximum strength of joint was 196 MPa. The optimum bonding parameters were: bonding temperature T= 830 ℃, bonding pressure p= 10 MPa and bonding time t= 30 min.

Key words: titanium alloy; tin-bronze; diffusion bonding; copper interlayer

Intelligent process modeling of robotic plasma spraying based on multi-layer artificial neural network XIA Weisheng[1,2], ZHANG Haiou[2], WANG Guilan[1], YANG Yunzhen[1] (1. State Key Laboratory of Material Processing and Die & Mould Technology, Huazhong Universiry of Technology, Wuhan 430074, China; 2. State Key Laboratory of Digital Manufacturing Equipment and Technology, Huazhong University of Science & Technology, Wuhan 430074, China). p 41—44

Abstract: The implementation of multi-layer artificial neural networks (ANNs) in robotic plasma spraying was discussed and an intelligent process model was constructed to fully describe the relationships between process parameters and coating properties. Influences of plasma arc current, spray distance, robot scanning space and scanning velocity on coating properties, i. e. residual stress and porosity, were systematically studied based on the present model. Prediction can be effectively carried out after the learning of the experimental database. Theoretical analysis shows the prediction results agree well with the experiments. It is favorable to fully investigate the complex and nonlinear relationships between processing parameters and coating properties as well as to overcome the limited information indicated by the discrete variable in the processing results.

Key words: robotic plasma spraying; artificial neural network; intelligent model; residual stress; porosity

Kinematics and track amendments of intersecting pipe welding robot DU Hongwang[1,2], WANG Zongyi[2], LIU Shaogang[1], ZHAO Yanan[1] (1. College of Mechanical & Electrical Engineering, Harbin Engineering University, Harbin 150001, China; 2. College of Automation, Harbin Engineering University, Harbin 150001, China). p 45—48

Abstract: According to the welding particularity on the junctions of intersecting pipe, the 4 degrees of freedom suspended welding robot was developed and mechanical structure of the body was introduced. Based on the relation of the joints, the kinematics modeling was established with the method of D-H (Denavit-Hartenberg). To overcome the size error and processing error and welding distortion, the welding track was taught in order to ensure welding quality, and then theory track was amended by the linear interpolation. According to the kinematics modeling, the simulation was carried out with SemMechanic. The results of experiments show that the welding quality meet the requirements actually.

Key words: welding robot; kinematics; teaching; linear interpolation

Dynamical simulation on the pressure response of load system of linear friction welding machine YIN Dongdong, DU Suigeng, YU Longqi, MA Yunfeng (Key Laboratory of Ministry of Education for Contemporary Design and Integrated Manufacturing Technology, Northwestern Polytechnical University, Xi'an 710072, China). p 49—52, 56

Abstract: In order to study the closed-loop control qualities of the electro-hydraulic servo load system of the linear friction welding machine on the slipway pressure, closed-loop transfer function of the pressure for the electro-hydraulic servo load system was established according to the relationship between input and output variables, a simulation model was established according to the transfer function and the simulation was carried out. In order to validate reliability of the simulation result, a frequency characteristics experiment of pressure was implemented under closed-loop control, and the system pressure's affect on the pressure's closed-loop response characteristics was specially analyzed. The results show as follows: the emulational and experimental results are anastomosing; the electro-hydraulic servo load system is a second-order inertial & first-order differential link for closed-loop pressure control, the system frequency width is large, and the system stability is high; pressure's closed-loop dynamic response characteristics can be improved by promoting the system pressure.

Key words: linear friction welding machine; electro-hydraulic servo system; dynamic quality; simulation

Study on rapid solidification welding techniques of quenched Cu-Sn alloy foils ZHAI Qiuya, YANG Jinshan, XU Jinfeng, GUO